coatings

MDPI

Article

Effect of Ultrasonic Impact on the Organization and Friction Wear Performance of AZ31B Magnesium Alloy Micro-Arc Oxidation Composite Coating

Qingda Li [1,*], Hao Wang [1], Canyu Che [2], Lin Wan [1], Xiaowei Dong [1], Song Wang [1] and Chong Zhang [1]

[1] College of Engineering, Heilongjiang Bayi Agricultural University, Daqing 163319, China; wh202097@163.com (H.W.); wanlin163@byau.edu.cn (L.W.); dxwai@byau.edu.cn (X.D.); wshbau@163.com (S.W.); 13753579100@163.com (C.Z.)

[2] Shanghai Institute of Ceramics, Chinese Academy of Sciences, Shanghai 200050, China; checanyu@163.com

* Correspondence: liqingda23@126.com

Abstract: To enhance the frictional wear performance of AZ31B magnesium alloy, a nanocrystalline layer was prepared by ultrasonic impact (UI) treatment on magnesium alloy samples, and the effects of different ultrasonic impact times (5 min, 10 min, and 15 min) on the organization and wear resistance of the composite coating were studied. The findings revealed that the maximum thickness of the composite coating was about 50 µm after 10 min of impact time, which was approximately 15 µm higher than that of the MAO coating. The elemental composition of the composite coating was mainly Mg, O, and Si elements, and the phase structure of the coating, mainly MgO and Mg_2SiO_4, was the same before and after UI. The microhardness value gradually decreased in a gradient with the increasing distance from the sample surface. The coating had a lower average coefficient of friction (0.18) and lower wear loss (1.56 mg) for the 15 min impact time. Moreover, a small amount of abrasive and adhesive wear served as the primary modes of wear.

Keywords: AZ31B magnesium alloy; ultrasonic impact; micro-arc oxidation; composite coating; friction wear performance

check for updates

Citation: Li, Q.; Wang, H.; Che, C.; Wan, L.; Dong, X.; Wang, S.; Zhang, C. Effect of Ultrasonic Impact on the Organization and Friction Wear Performance of AZ31B Magnesium Alloy Micro-Arc Oxidation Composite Coating. *Coatings* **2023**, *13*, 1161. https://doi.org/10.3390/coatings13071161

Academic Editor: Petr M. Pivkin

Received: 21 May 2023
Revised: 4 June 2023
Accepted: 21 June 2023
Published: 27 June 2023

Copyright: © 2023 by the authors. Licensee MDPI, Basel, Switzerland. This article is an open access article distributed under the terms and conditions of the Creative Commons Attribution (CC BY) license (https://creativecommons.org/licenses/by/4.0/).

1. Introduction

Magnesium alloy is the lightest metal in all engineering materials; its density is 1.74 g/cm^3, only two-thirds of the density of aluminum alloy, and it is specifically strong and specifically stiff, with the same stiffness as aluminum alloy but with a weight reduction of about 25% [1–3]. Magnesium alloy has good anti-shock and noise reduction performance, and, when magnesium alloy is impacted by external forces, the energy that can be absorbed in the elastic range is twice that of aluminum alloy [4,5]. In addition, the strong electromagnetic shielding ability, good thermal conductivity, and excellent cutting and processing properties of magnesium alloy make it have broader application prospects in the electronics industry, the aerospace industry, the automotive industry, and other fields [6,7]. However, there are still many difficulties in the practical application of magnesium alloys. For example, the hardness of magnesium alloy is low, which makes it difficult to withstand the basic dynamic load, so it can only be used to manufacture static load parts. Magnesium alloy has poor high temperature creep resistance, so, once its working environment temperature is too high, magnesium alloy's resistance to overheating is greatly reduced, which means magnesium alloy can only work for a long time in the field with low temperature and a low stress risk. Magnesium alloy is easy to deform because of its plasticity, and its wear resistance is poor, which severely limits the use of magnesium alloys in machinery [8,9]. Given this, finding a suitable method to improve the properties of magnesium alloys is the key to promoting the further development of magnesium alloys. At present, some scholars at home and abroad often use surface treatment technologies such as overlay welding,

cladding, spraying, chemical heat treatment, and micro-arc oxidation to improve the wear resistance of mechanical parts [10–14].

Micro-arc oxidation (MAO) is an important electrochemical surface treatment technology that uses environmentally friendly weak alkaline and acidic electrolytes to produce thick, hard, dense ceramic coatings on the surface of various valve metals (e.g., magnesium, aluminum, and titanium) by generating strong electric sparks in the electrolyte through high temperature and high-pressure action. This technology, compared to traditional surface treatment technologies, has the advantages of environmental protection, simple operation, a stable process, etc. The resulting coatings have good frictional, corrosive, electrical, and thermal properties and are widely used in machinery, aerospace, aircraft, automobiles, biomedical devices, etc. [15,16]. However, as science and technology continue to evolve, the demands placed on materials in industrial production are increasing, so it is challenging to meet the needs of the long-term use of materials such as valve metals under complex working conditions using a single MAO technology. For many years, researchers have been trying to combine MAO technology with other surface treatment technologies to enhance the performance of the coating. Tazegul et al. [17] used a cold spray method to deposit aluminum powder on the surface of AZ91D magnesium alloy, followed by micro-arc oxidation to form a new alumina layer. The results showed that the new coating exhibited good wear resistance with improved hardness and a bonding-force-reduced average friction coefficient, and the wear rate compared to that of the single MAO coating. However, since cold spraying mainly relies on the kinetic energy of the particles moving at high speed to impact the substrate and, thus, deposit the coating on the metal surface; this makes it difficult to deposit this technique on many brittle material surfaces.

In recent years, surface nanocrystallization technology has become a hot research topic for domestic and foreign scholars. Surface Mechanical Attrition Treatment (SMAT), ultrasonic impact (UI), High Energy Shot Peening (HESP), and other surface treatment technologies can make the metal surface undergo intense plastic deformation, which leads to the gradient nanostructure layer by gradually refining the coarse crystals to nanocrystals on the material surface, and this nanostructure layer can effectively improve the atomic kinetic diffusion performance and chemical reaction rate [18–20]. Ren et al. [21] used HESP to prepare nanosized coatings on the surface of TC4 titanium alloy by surface pretreatment, which was treated with MAO to obtain composite ceramic coatings. The outcomes demonstrated that the HESP-treated composite coating's friction coefficient was lower and more stable than that of the MAO coating, and the wear rate decreased by about 71.3%. Masiha et al. [22] prepared a composite coating on AA1230 aluminum alloy using SMAT + MAO technology. The authors' findings indicated that samples treated with SMAT for nine hours had a lower friction coefficient than samples treated for three hours, and the increase in SMAT process duration had little effect on the thickness of the nanocrystalline layer but a greater effect on the number of nanoparticles present in the coating, which was the main reason for the decrease in the friction coefficient. Gheytani et al. [23] performed surface nanosizing of AZ31B magnesium alloy by SMAT technology in MAO electrolyte with the addition of alumina nanopowder and the MAO process. According to the findings, the composite coating's wear resistance rose by a maximum of 105%, when compared to the single MAO coating's wear resistance. Observing the surface morphology, it is evident that the surface mechanical abrasive treatment facilitated the coating's uptake of nanoparticles, which led to a substantial improvement in the wear resistance of the coating. In summary, the composite process of the surface nanocrystallization process combined with the micro-arc oxidation process has a very significant effect on improving the surface friction wear performance of the material surface. However, the current surface nanotreatment equipment is generally expensive, is inconvenient to operate, and has other disadvantages. Ultrasonic impact equipment is a good remedy for these defects, which has the advantages of easy operation, high efficiency, a low cost, and flexible applicability. The prepared UI–MAO composite coating can be closely bonded with the substrate and has excellent properties. However, to date, many scholars have usually focused on the degree

of improvement of the properties of the prepared composite coatings compared to those of single coatings, while relatively little research has been conducted on how the performance of MAO coatings is affected by the amount of time of the self-nanosizing treatment of the material surface.

Given this, in this study, a composite process combining the ultrasonic impact treatment process and the MAO process was used to prepare an MAO composite coating on the surface of AZ31 magnesium alloy to improve the wear resistance of magnesium alloy, the effects of different UI process times (5 min, 10 min, and 15 min) on the microstructure and frictional wear properties of the composite coating were investigated, and the frictional wear mechanism was revealed. To expand the further application of the UI treatment process in the field of material surface wear treatment, this study provides the scientific and theoretical basis.

2. Materials and Methods

2.1. Preparation of the Composite Coating

This experiment selected AZ31B magnesium alloy (Han Yong Metal Material Company, Dongguan, China) as the substrate material. The composition is shown in Table 1; the substrate is EDM-cut into 20 mm × 40 mm × 5 mm samples; and the AZ31B magnesium alloy substrate, in turn, is coarsely to finely ground with 400#, 800#, 1200#, and 1500# water-resistant sandpaper until the surface is smooth, to ensure that the samples have the same surface roughness. After each experiment, the samples should be rinsed with acetone, anhydrous ethanol solution, and deionized water, in turn; dried by a hair dryer; and then preserved and packed in sealed bags.

Table 1. Chemical composition of AZ31B (wt%).

Al	Zn	Mn	Si	Fe	Cu	Ni	Mg
2.96	0.52	0.31	0.16	0.003	0.006	0.001	Balance

The AZ31B magnesium alloy samples were treated with UI equipment (HI-T002015A, Hightower, Handan, China), and the surface of the samples was made to undergo plastic deformation by the reciprocal impact of the impact head on the surface of the samples [24]. The specific test parameters were impact amplitude 25 μm, impact frequency 30 KHz, input current 0.2 A, single head impact, impact head diameter 6 mm, and impact head travel speed 5 mm/s. According to a related study by Chen et al. [25], it was found that when the ultrasonic impact time was 5 min, 10 min, and 15 min, a better plastic deformation layer appeared on the material surface, and the grain refinement was obvious. Therefore, the impact head continuously impacted the surface of the magnesium alloy for 5 min, 10 min, and 15 min. The samples were prepared by micro-arc plasma oxidation and integrated polishing equipment (HT1001P, Harbin, China) with UI–MAO composite coating (Figure 1). In the MAO process, the stainless steel plate served as the cathode, and the substrate served as the anode. The current intensity was 12 A/dm^2, the duty cycle was 10%, the frequency was 1000 HZ, and the oxidation time was 10 min. The micro-arc oxidation electrolyte system consisted of 10 g/L Na_2SiO_3, 4 g/L NaOH, and 2 g/L $(NaPO3)_6$. To keep the temperature below 30 °C throughout the test, the electrolyte was constantly mixed and chilled.

2.2. Microstructure Characterization

The surface morphology and cross-sectional morphology of the samples were examined using a scanning electron microscope (EM-30AX+, COXEM, Daejeon, Korea) at an operating voltage of 30 kV, a resolution of 5 nm, and a magnification of 15~150,000 times. In this experiment, before observing the microscopic morphology, the sample should be sprayed with gold to make it conductive, and, before observing the cross-section, the sample should be inlaid, encapsulated, leaving only the observation surface, then polished, and sprayed with gold. The sample surface was spot-scanned using an energy spectrome-

ter attached to a scanning electron microscope (Xplore compact 30, Oxford Instruments, Oxford, UK) in order to determine the sample's elemental composition. The surface and cross-sectional microhardness of the samples were measured using a digital Vickers hardness tester (TMVS-1, Shenzhen, China) by applying a load of 9.8 N for 15 s. Five points at 2 mm intervals were selected for measuring the surface hardness of the samples, and the results were averaged; the cross-sectional direction was measured at 5 μm intervals, and the results were averaged. The thickness of the MAO coating was measured using a coating thickness gauge (Salu Tron D3, Siltronic, Munich, Germany) with a range of 0~3000 μm, resolution of 0.1 nm, and rated voltage of 9 V. To reduce the measurement error caused by the unevenness of the surface of the MAO coating, the coating surface was randomly measured 10 times using the instrument, and the effective thickness was determined by averaging the results of the 10 measurements. To describe the phase structure of the magnesium alloy samples, an X-ray diffractometer (D8 advance, Bruker, Karlsruhe, Germany) was utilized with a voltage of 40 kV, a current adjustment of 30 mA, a diffraction angle scan range of 20°–90°, a scan step of 0.02°, and a scan rate of 5°/min; K rays from Cu targets were used. A microcomputer-controlled end-face friction and wear tester (MMU-10, Zhong Yi, Jinan, China) was used to conduct each friction and wear test, and the ball-disk friction substrate was selected for the study, in which the friction substrate was a small Si_3N_4 ball of 5 mm diameter, the load was 5 N, the speed was 150 r/min, and the friction time was 600 s. A microscopic precision electronic balance (WANTE, Wante, Hangzhou, China) was selected to measure the sample wear weight loss, and the measurement accuracy is 0.001 g, due to the small weight loss of the sample after the friction and wear experiment. To ensure the accuracy of the experiment, it is necessary to use anhydrous ethanol to ultrasonically clean the sample after the wear test and wait to use a hair dryer to dry before weighing. After the friction wear test, the sample surface's wear morphology was examined under a scanning electron microscope.

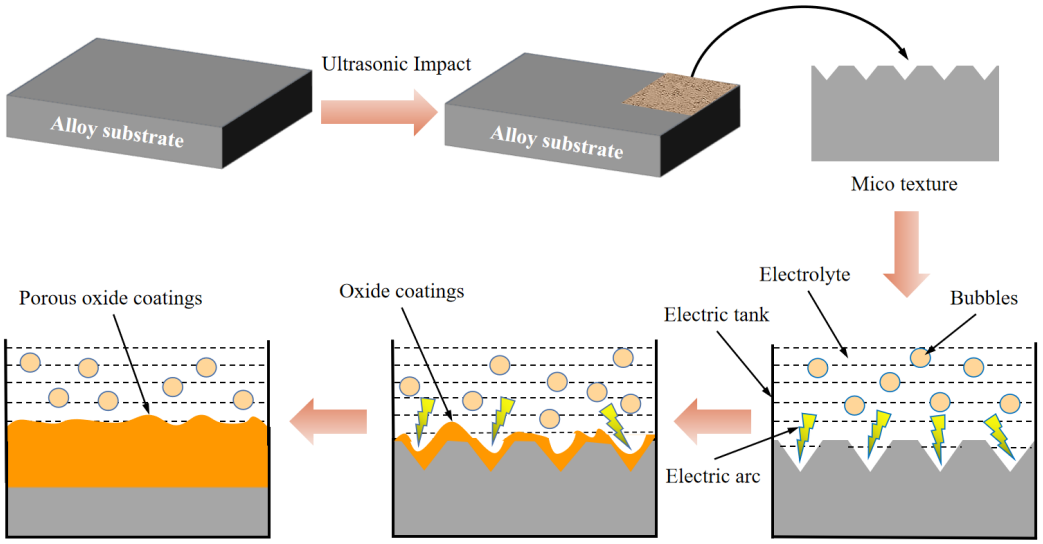


Figure 1. Schematic diagram of the preparation principle of UI–MAO composite coating.

3. Results and Discussion

3.1. Surface Morphologies of the Coatings

The SEM morphologies of the UI–MAO composite coating at various impact periods are depicted in Figure 2. From Figure 2a, it is evident that the AZ31 magnesium alloy's surface is abrasive and porous following the MAO process, and the pore size varies; like a crater, the edge is raised, and the central cavity is depressed. When the molten reaction material is discharged down the discharge channel within the discharge microzone during the MAO process, it leaves behind this porous structure as a trace of the discharge channel residue and is rapidly cooled and solidified by the electrolyte [26,27]. In addition,

Figure 2b demonstrates that the impact process has a very noticeable impact on the surface morphology of the oxide film and that the impact method results in coating surfaces that are less porous than those produced by the MAO approach; the microporous size gradually decreases with the growth of the impact time, indicating that the UI process can inhibit the sprouting and development of MAO coatings [28]. As can be seen, the MAO coating's surface pores have an erratic form and range in size, while the pores of the UI-treated composite coating are almost uniform in size and are relatively rounded in shape. With the increase in impact time, as shown in Figure 2c,d, the size of the coating holes no longer changed, and a few tiny cracks started to appear around the micro-hole structure on the coating surface. The main reason is that the UI process refines the metal surface grains, forms nanocrystalline layers, and has more defect points, which makes the substrate easier to accelerate discharge during the MAO process, to the extent that more discharge channels are formed [29,30]. Additionally, the prolonged impact period may result in the presence of residual strains on the substrate's surface, and these remaining tensions cause the coating's surface to develop minute fissures.

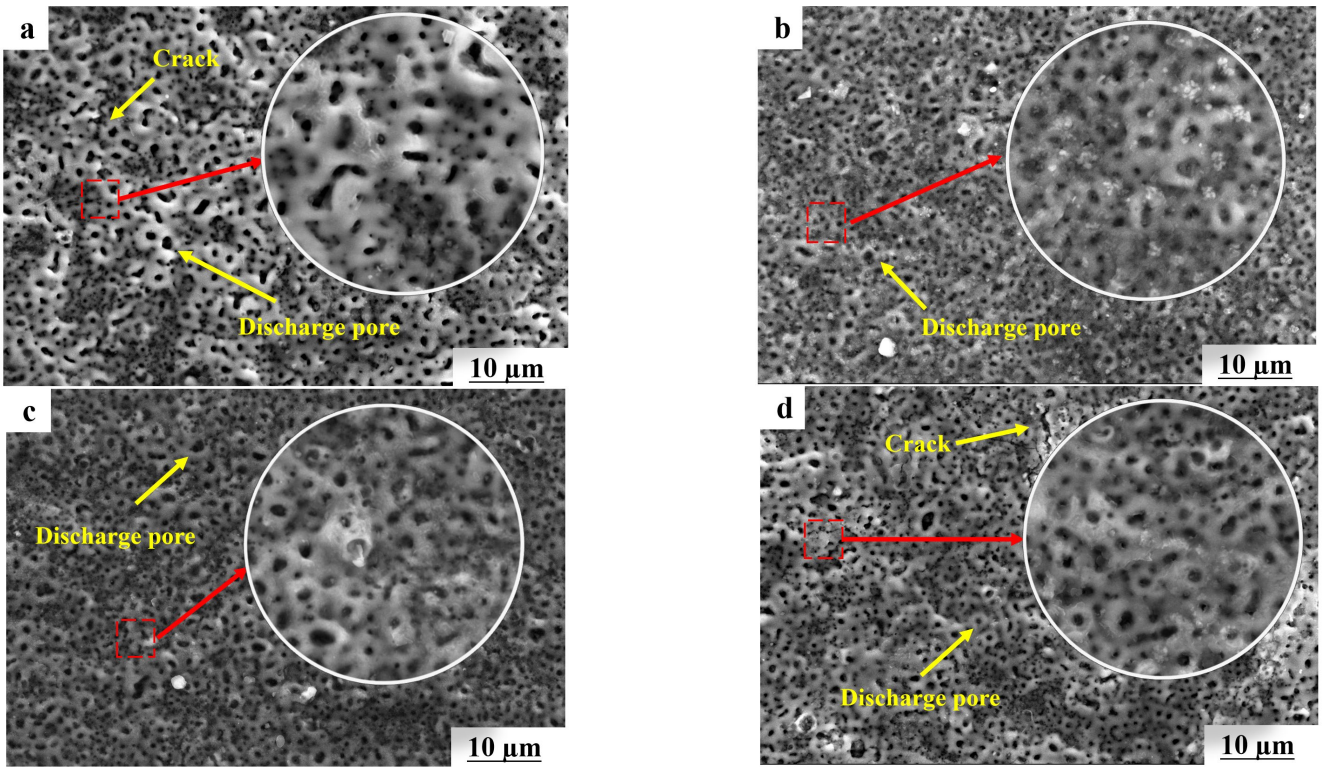


Figure 2. Surface morphologies of the coatings prepared using different UI process times: (**a**) 0 min, (**b**) 5 min, (**c**) 10 min, and (**d**) 15 min.

3.2. Cross-Sectional Morphologies of the Coatings

Figure 3 illustrates the MAO coating's cross-sectional morphology over multiple impact times. Figure 3a shows that the MAO coating and substrate have a canine teeth interwoven structure and that the MAO coating is relatively compact and well-bonded to the substrate, with a coating thickness of about 35 μm. The surface of the coating shows obvious cross-mixed microcracks, which result from the discharge channels created during the MAO process by the electric spark discharge. From Figure 3b–d, compared to the single MAO coating, the MAO composite coating has a thickness of about 46 μm after 5 min of impact, and the UI–MAO composite coating's surface exhibits numerous small cracks, which are uniformly distributed and longitudinal between the coating and the substrate. With the extension of the impact time to 10 min, these cracks become more detailed and denser, and the thickness of the UI–MAO composite coating at this time is around 50 μm.

The cause is the tiny grains left behind from the UI process on the metal's surface that encourage the metal's breakdown in the MAO process, making the discharge process more uniform and continuous, which accelerates the growth rate of the coating, on the one hand, and promotes the growth of the thickness, on the other hand. This proves that the UI process contributes to the enhancement of the MAO coating. However, the coated surface develops pits and cracks after 15 min of contact, and the coating thickness also decreases to about 48 µm. This is due to the uneven distribution of the nanocrystalline layers on the substrate surface due to long-time impact, which hinders the spark discharge of MAO [31].

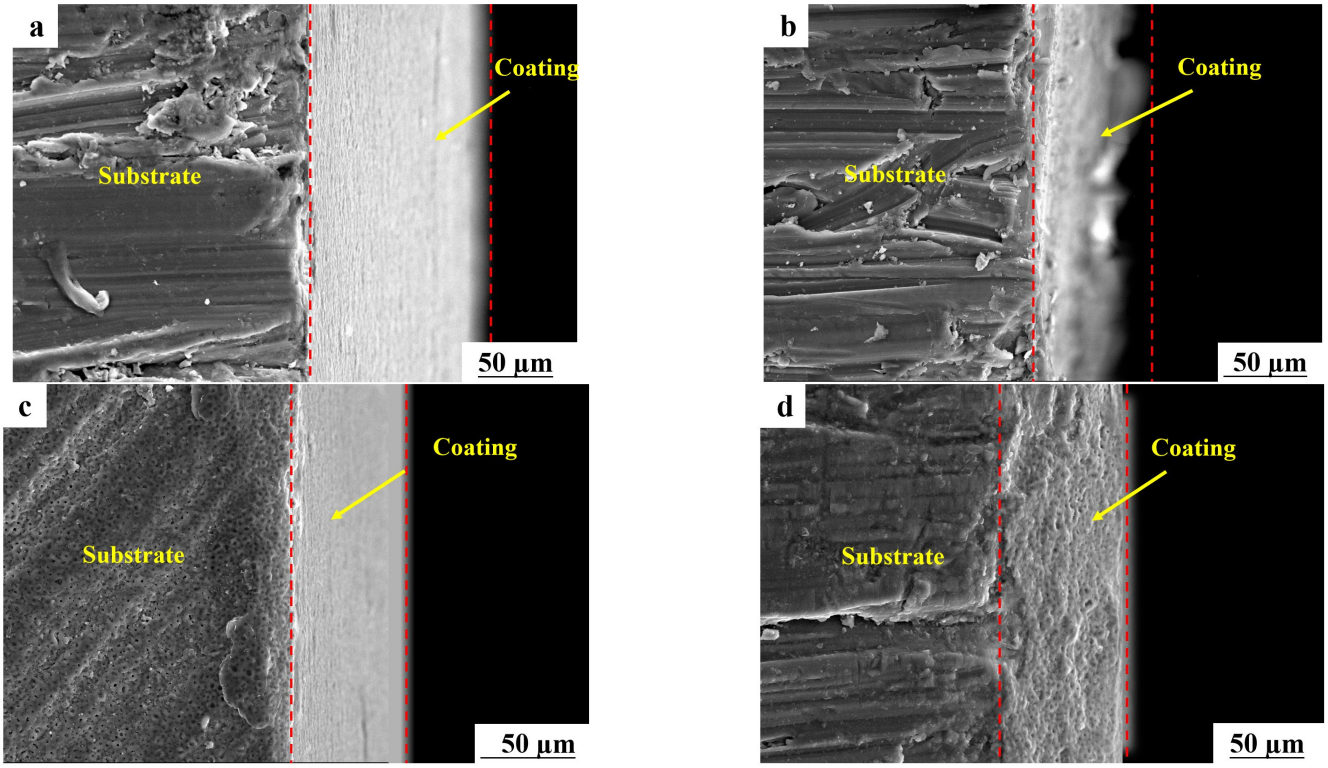


Figure 3. Cross-sectional morphologies of the coatings prepared using different UI process times: (**a**) 0 min, (**b**) 5 min, (**c**) 10 min, and (**d**) 15 min.

3.3. Phase Composition of the Coatings

The EDS elemental analysis of the MAO coatings, both before and after the UI procedure, is shown in Figure 4. By comparing Figure 4b–d with Figure 4a, it is found that the elemental composition of the UI + MAO composite coating is dominated by Mg, O, and Si elements and also contains small amounts of Na, Al, C, and P. When compared to the MAO coating, the elemental makeup of the composite coating is not considerably different. However, the elemental content of Mg and O in the composite coating increased compared to that before treatment, and the elements increased with the extension of the impact time. This suggests that the UI procedure encouraged the magnesium alloy substrate's film-forming reaction during the MAO process.

Figure 5 displays the XRD patterns of the MAO coatings at various impact periods. As can be observed, MgO and Mg_2SiO_4 make up the majority of the coatings, and the main phase composition of the coatings does not significantly change depending on the impact duration, which indicates that the UI process does not change the phase structure of the coatings. The production of Mg_2SiO_4 also proves that the components of the electrolyte are also involved in the film formation reaction. The longer the coating's impact duration is, the higher the diffraction peak value is and the more MgO and Mg_2SiO_4 there are in the coating, which indicates that the nanocrystalline layer produced by the UI process promotes the

MAO film formation reaction. The longer the impact time is, the more significant the grain refinement effect is, and the more it promotes the MAO process reaction.

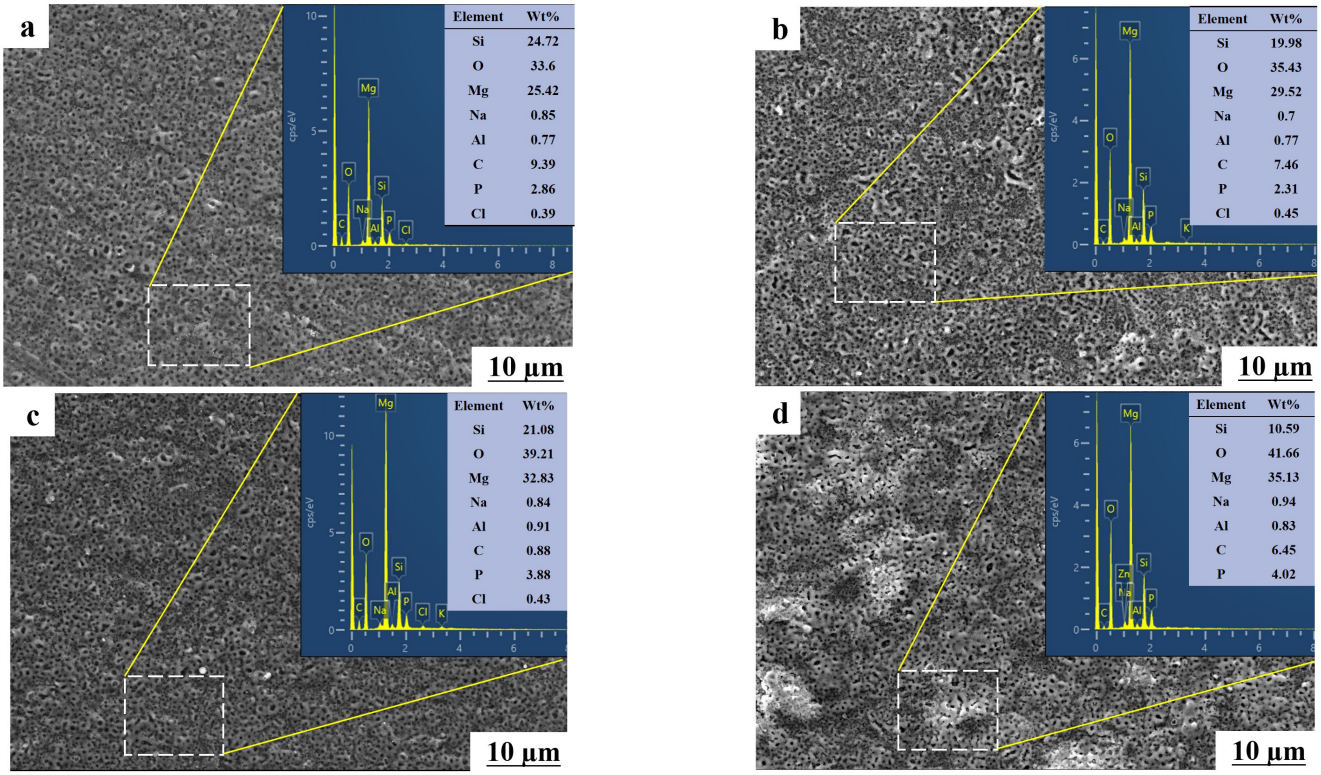


Figure 4. EDS maps of the coatings prepared using different UI process times: (**a**) 0 min, (**b**) 5 min, (**c**) 10 min, and (**d**) 15 min.

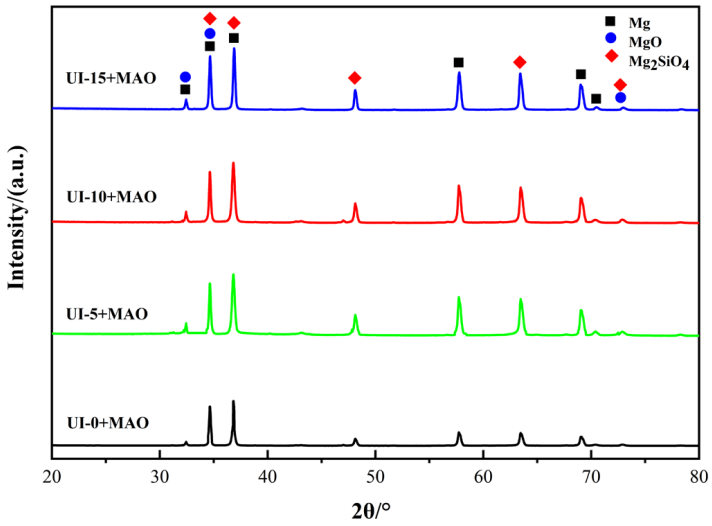


Figure 5. XRD patterns of the coatings prepared using different UI process times.

3.4. Microhardness of the Coatings

Figure 6 displays the coating microhardness distribution curves along the depth for various impact times. It is evident that the single MAO coating has a surface hardness of 160.26 HV, and the AZ31 substrate has a surface hardness of 81.46 HV, while the surface hardness of the sample after 5 min of the impact process reaches 196.33 HV, which is approximately 2.5 times that of the substrate. The surface hardness after 10 and 15 min

of impact is 196.71 HV and 226.23 HV, respectively, which increases with the increase in impact time. According to the Hall–Petch equation:

$$H = H_0 + k\sqrt{d} \quad (1)$$

where k is a constant for a particular substance, H_0 is a suitable constant related to the hardness measurements, and d is the average particle size. This relationship was demonstrated in numerous metallic materials with grain sizes in the micrometer range, both in theory and in fact [32]. It can be seen that the hardness of the metal materials is inversely proportional to the grain size. The surface grains of the sample were refined during the UI process, increasing the sample's surface hardness. The extension of the impact time further refined the grains and increased the hardness of the sample [33]. As the sample's distance from the surface increased, the hardness value gradually showed a gradient downward trend, and, finally, about 50 µm from the surface of the sample it tended to level off and finally reached the matrix hardness.

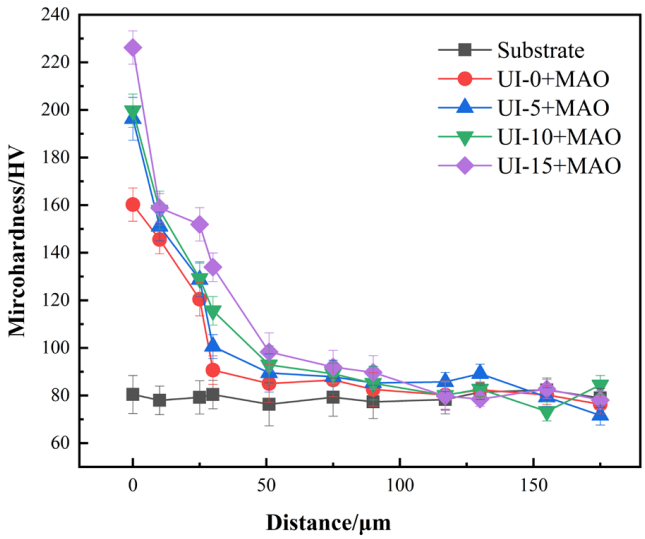


Figure 6. Microhardness of the coatings prepared using different UI process times.

3.5. Friction Coefficient of the Coatings

Figure 7 displays the plot of the coefficient of friction vs. time for each specimen following the friction wear test. The coefficient of friction of the AZ31 substrate was the highest, and the overall coefficient of friction fluctuated, with an average coefficient of friction of 0.38 and a maximum wear loss of 5.25 mg (Figure 8). The dynamic coefficient of friction of the single MAO coating fluctuated between 0.31 and 0.36 after the initial run and stage, with an average coefficient of friction of 0.34. The wear loss was 4.63 mg, which was about 0.88 times that of the substrate's wear loss. The friction coefficient of the specimens after the UI process was reduced, compared with that before the treatment, after the initial run and stage, and the lowest friction coefficient was found for the specimens with 15 min of the UI process, with an average friction coefficient of 0.18. The lowest wear weight loss was 1.56 mg, which was about 0.29 times the substrate's wear amount. This shows that the composite coating treated by the UI process is more effective in enhancing the wear resistance of the substrate. This is due to the fine-grained strengthening effect of the UI process, which improves the surface roughness and hardness of the specimen, reduces the strength of the cold-welded junction during the friction process, which, in turn, reduces the adhesion of the specimen surface and makes the specimen more wear-resistant [34].

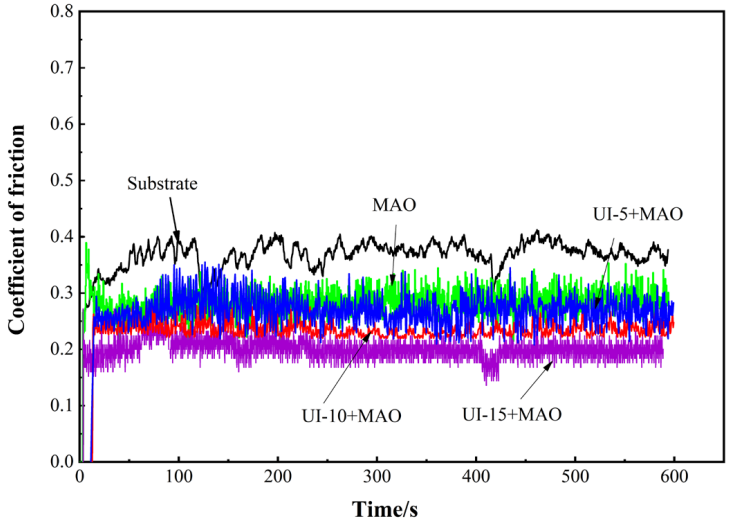


Figure 7. Coefficient of friction of the coatings prepared using different UI process times.

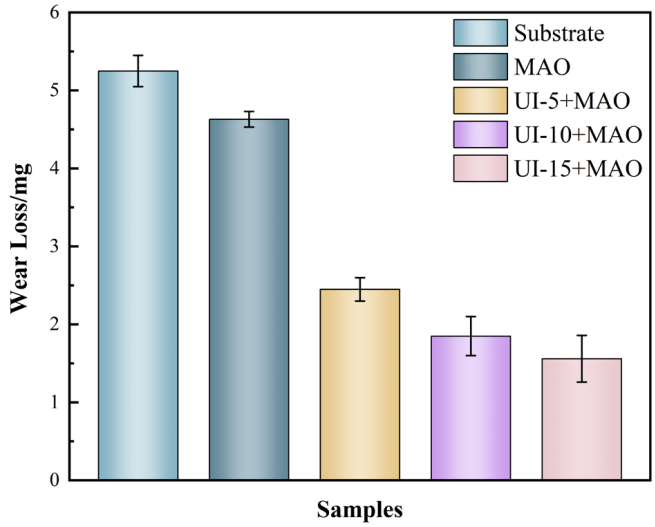


Figure 8. Wear loss of the coatings prepared using different UI process times.

3.6. Wear Morphologies of the Coatings

The surface microscopic wear morphology of each sample following the friction wear test is shown in Figure 9. It is clear from Figure 9a that there are many deep and shallow scratches, similar to ploughings, on the surface of the AZ31 substrate, that there are more wear particles and craters on the sample's surface, and that the sample's surface is more severely worn. This is because the hardness of the Si_3N_4 spheres is higher than that of the sample during the frictional wear process. As the frictional sliding proceeds, the shear force at the bonding point gradually increases, resulting in the formation of wear particles, which, in turn, generates grooves with the surface of the substrate and eventually causes abrasive wear. Therefore, the wear mechanism of the AZ31 substrate surface is reported to be mostly adhesive wear with abrasive wear [35–38]. Figure 9b shows the microscopic appearance of wear on the surface of the MAO coating. The oxide layer on the surface of the coating is worn through, producing many ploughings that are parallel to the friction direction and a slight plastic deformation at the same time, which results from the MAO coating's surface's pore structure and significant roughness, which generates large shear stress at the contact point when abrasion occurs with the counter-abrasive ball, thus wearing through the MAO coating. In addition, plastic deformation is produced by shear stress [39,40]. Therefore, the wear mechanism of the MAO coating evolves mainly as abrasive wear, accompanied by

slight adhesive wear. From Figure 9c, when the number of ploughings on the surface of the composite coating after 5 min of impact becomes less compared to that of the single MAO coating, accompanied by a small number of wear particles, this phenomenon becomes more obvious after 10 min of impact (Figure 9d), and the main, exhibited wear mechanisms are minor abrasive wear and adhesive wear [41]. In addition, when the impact time was 15 min, as shown in Figure 9e, the shallowest abrasion marks of the composite coating appeared at this time, and the ploughings were flatter. This may be because the gradient nanocrystalline layer formed on the surface of the magnesium alloy can effectively block the contact between the substrate and the friction substrate, thus slowing down the degree of wear on the surface of the specimen. After 15 min of impact, only slight adhesive wear accompanied by slight abrasive wear occurred in the composite coating [42].

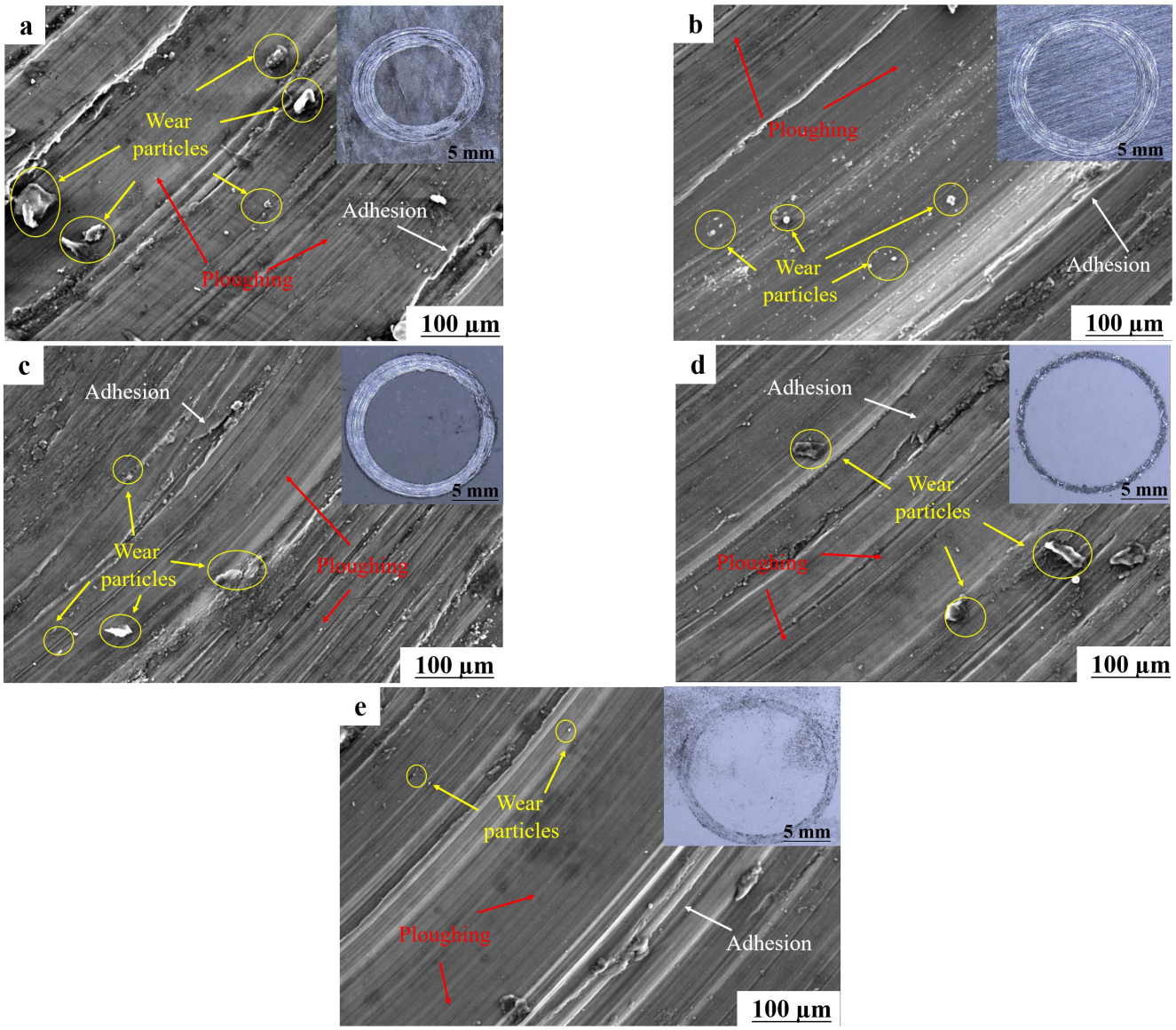


Figure 9. Wear morphologies of the coatings prepared using different UI process times: (**a**) substrate, (**b**) 0 min, (**c**) 5 min, (**d**) 10 min, and (**e**) 15 min.

4. Conclusions

In this study, the aim was to solve the problem of the poor wear resistance of magnesium alloy itself and to extend its application in different fields. On the surface of AZ31 magnesium alloy, UI–MAO composite coatings were created by combining the

MAO process and the UI process. A comparative study on the organization and frictional wear properties of the coatings under different UI process times was carried out, and the subsequent deductions were made.

(1) The MAO composite coating's thickness was enhanced by the UI process, reaching a maximum of about 50 μm at a 10 min impact time. Without the UI process, the MAO coating's thickness was about 35 μm, so it increased by about 15 μm.
(2) The phase structures of the MAO coatings before and after the UI process were the same, both mainly composed of MgO and Mg_2SiO_4, but the increase in impact time caused the content of MgO and Mg_2SiO_4 to rise, which promoted the film formation reaction of the MAO process.
(3) With a UI process time of 15 min, the surface microhardness of the UI–MAO composite coating peaked at 226.23 HV, which was roughly 2.5 times that of the AZ31 base material. With increasing distance from the sample's surface, the microhardness value gradually displayed a decreasing gradient trend.
(4) With the lowest average coefficient of friction and wear amount of 0.18 and 1.56 mg, respectively, after 15 min of impact, the UI–MAO composite coating had superior wear resistance compared to the MAO coating. Small amounts of adhesive and abrasive wear together constitute the primary wear mechanism.

Author Contributions: Conceptualization, Q.L. and H.W.; methodology, H.W.; validation, H.W. and C.C.; formal analysis, H.W.; investigation, Q.L.; resources, Q.L.; data curation, L.W.; writing—original draft preparation, X.D.; writing—review and editing, S.W.; visualization, C.Z.; supervision, H.W.; project administration, Q.L.; funding acquisition, H.W. All authors have read and agreed to the published version of the manuscript.

Funding: This work was financially supported by the Natural Science Foundation of Heilongjiang Province of China (No. LH2022E098) and the Heilongjiang Bayi Agricultural University Support Program for San Zong (No. ZDZX202102).

Institutional Review Board Statement: Not applicable.

Informed Consent Statement: Not applicable.

Data Availability Statement: Not applicable.

Conflicts of Interest: The authors declare no conflict of interest.

References

1. Li, T.; Leng, Z.J.; Wang, X.T.; Wang, S.F.; Zhang, S.Q.; Yang, Y.S.; Zhou, J.X. Microstructure and electrical conductivity of electroless copper plating layer on magnesium alloy micro-arc oxidation coating. *Trans. Nonferrous Met. Soc. China* **2022**, *32*, 3950–3962. [CrossRef]
2. Saberi, A.; Bakhsheshi-Rad, H.R.; Abazari, S.; Ismail, A.F.; Sharif, S.; Ramakrishna, S.; Daroonparvar, M.; Berto, F. A Comprehensive Review on Surface Modifications of Biodegradable Magnesium-Based Implant Alloy: Polymer Coatings Opportunities and Challenges. *Coatings* **2021**, *11*, 747. [CrossRef]
3. Song, J.F.; She, J.; Chen, D.L.; Pan, F.S. Latest research advances on magnesium and magnesium alloys worldwide. *J. Magnes. Alloys* **2020**, *8*, 1–41. [CrossRef]
4. Liu, C.; Zhang, W.; Xu, T.L.; Hong, T.; Jiang, B.L.; Miao, X. Preparation and corrosion resistance of a self-sealing hydroxyapatite-MgO coating on magnesium alloy by microarc oxidation. *Ceram. Int* **2022**, *48*, 13676–13683. [CrossRef]
5. Bakhsheshi-Rad, H.R.; Hamzah, E.; Ismail, A.F.; Aziz, M.; Daroonparvar, M.; Saebnoori, E.; Chami, A. In vitro degradation behavior, antibacterial activity and cytotoxicity of TiO-MAO/ZnHA composite coating on Mg alloy for orthopedic implants. *Surf. Coat. Technol.* **2018**, *334*, 450–460. [CrossRef]
6. Sikdar, S.; Menezes, P.V.; Maccione, R.; Jacob, T.; Menezes, P.L. Plasma Electrolytic Oxidation (PEO) process—Processing, properties, and Applications. *Nanomaterials* **2021**, *11*, 1375. [CrossRef] [PubMed]
7. Fattah-Alhosseini, A.; Chaharmahali, R.; Babaei, K. Effect of particles addition to solution of plasma electrolytic oxidation (peo) on the properties of peo coatings formed on magnesium and its alloys: A review. *J. Magnes. Alloys* **2020**, *8*, 799–818. [CrossRef]
8. Józef, I.; Monika, S. Microstructure and corrosion resistance of AZ91 Magnesium Alloy after Surface Remelting Treatment. *Materials* **2022**, *24*, 15.
9. Yao, W.H.; Wu, L.; Wang, J.F. Micro-arc oxidation of magnesium alloys: A review. *J. Mater. Sci. Technol.* **2022**, *118*, 158–180. [CrossRef]

10. Zhou, Z.L.; Yuan, W.H.; Fang, T.H.; Fu, Q. High temperature wear resistance of cobalt-Based cladding layer surfacing on H13 steel. *Key Eng. Mater.* **2019**, *815*, 81–88. [CrossRef]
11. He, B.F.; Ma, D.Y.; Ma, F.; Xu, K. Microstructures and wear properties of TiC coating produced by laser cladding on Ti-6Al-4V with TiC and carbon nanotube mixed powders. *Ferroelectrics* **2019**, *547*, 217–225. [CrossRef]
12. Zhang, L.Y.; Yang, S.M.; Lv, X.; Jie, S.H. Wear and corrosion resistance of cold-sprayed Cu-based composite coatings on magnesium substrate. *J. Therm. Spray Technol.* **2019**, *28*, 1212–1224. [CrossRef]
13. Kusmanov, S.A.; Tambovskiy, I.V.; Korableva, S.S.; Dyakov, I.G.; Burov, S.V.; Belkin, P.N. Enhancement of wear and corrosion resistance in medium carbon steel by plasma electrolytic nitriding and polishing. *J. Mater. Eng. Perform.* **2019**, *28*, 5425–5432. [CrossRef]
14. Zhu, Y.Y.; Chang, W.H.; Zhang, S.F.; Song, Y.W.; Huang, H.D.; Zhao, R.F.; Li, G.Q.; Zhang, R.F.; Zhang, Y.J. Investigation on corrosion resistance and formation mechanism of a P-F-Zr contained micro-arc oxidation coating on AZ31B magnesium alloy using an orthogonal method. *Coatings* **2019**, *9*, 197. [CrossRef]
15. Kaseem, M.; Fatimah, S.; Nashrah, N.; Ko, Y.G. Recent progress in surface modification of metals coated by plasma electrolytic oxidation: Principle, structure, and performance. *Prog. Mater. Sci.* **2020**, *117*, 100735. [CrossRef]
16. Wang, Z.C.; Zhao, H.; Zhang, Y.; Shi, X.Q.; Rao, M.S.; Wu, S.K. Effect of Voltage on the Microstructure and High-Temperature Oxidation Resistance of Micro-Arc Oxidation Coatings on AlTiCrVZr Refractory High-Entropy Alloy. *Coatings* **2022**, *13*, 14. [CrossRef]
17. Tazegul, O.; Muhaffel, F.; Meydanoglu, O.; Baydogan, M.; Kayali, E.S.; Cimenoglu, H. Wear and corrosion characteristics of novel alumina coatings produced by micro arc oxidation on AZ91D magnesium alloy. *Surf. Coat. Technol.* **2014**, *258*, 168–173. [CrossRef]
18. Wang, S.F.; Li, H.Q.; Chen, X.; Chi, J.; Li, M.; Chai, L.; Xu, H. Improving microstructure and wear resistance of plasma clad Fe-based alloy coating by a mechanical vibration technique during cladding. *Mater. Sci. Eng. A* **2010**, *528*, 397–401. [CrossRef]
19. Wang, P.F.; Han, Z.; Lu, K. Enhanced tribological performance of a gradient nanostructured interstitial free steel. *Wear* **2018**, *402–403*, 100–108. [CrossRef]
20. Sahu, J.N.; Sasikuma, C. Development of hard and wear resistant surface coating on Ni-Cr-Mo steel by surface mechano-chemical carburization treatment (SMCT). *J. Mater. Process. Technol.* **2018**, *263*, 285–295. [CrossRef]
21. Ren, C.; Luo, J.M.; Chen, Y.H.; Huang, J.; Xu, J.L. Effect of Shot Peening on Wear and Corrosion Behavior of Micro-arc Oxidation Coating of TC4 Alloy. *Mater. Rep.* **2020**, *34*, 18081–18085.
22. Masiha, H.R.; Bagheri, H.R.; Gheytani, M.; Aliofkhazraei, M. Effect of surface nanostructuring of aluminum alloy on post plasma electrolytic oxidation. *Appl. Surf. Sci.* **2014**, *317*, 962–969. [CrossRef]
23. Gheytani, M.; Bagheri, H.R.; Masiha, H.R.; Aliofkhazraei, M.; Sabour Rouhaghdam, A.; Shahrabi, T. Effect of SMAT preprocessing on MAO fabricated nanocomposite coating. *Surf. Eng* **2014**, *30*, 244–255. [CrossRef]
24. Yu, J.H.; Lee, K.Y.; Shim, D.S.; Park, S.H. Metal embedding and ultrasonic nanocrystal surface modification technology for super wear-resistant mechanical parts. *Int. J. Adv. Manuf. Technol.* **2019**, *101*, 951–962. [CrossRef]
25. Chen, F.R.; Yang, Y.H.; Li, N. Effect of ultrasonic impact time on microstructure and properties of 7A52 aluminum alloy tandemmig welded joint. *Int. J. Adv. Manuf. Technol.* **2021**, *116*, 2687–2696. [CrossRef]
26. Yu, S.; Zeng, D.P.; Zhu, H.; Zhang, W.; Wang, L.; Yu, Z.T.; Huo, W.T.; Guo, D.G.; Zhang, M.L.; Wang, G. Improvement on biocompatibility and corrosion resistance of a Ti3Zr2Sn3Mo25Nb alloy through surface nanocrystallization and micro-arc oxidation. *J. Mater. Sci.* **2022**, *57*, 5298–5314. [CrossRef]
27. Muhaffel, F.; Cimenoglu, H. Development of corrosion and wear resistant micro-arc oxidation coating on a magnesium alloy. *Surf. Coat. Technol.* **2018**, *357*, 89. [CrossRef]
28. Gu, Y.; Ma, H.; Yue, W.; Tian, B.; Chen, L.; Mao, D. Microstructure and corrosion model of MAO coating on nano grained AA2024 pretreated by ultrasonic cold forging technology. *J. Alloys Compd.* **2016**, *681*, 120–127. [CrossRef]
29. Zhu, B.; Wang, L.; Wu, Y.; Liang, J.; Cao, B.C. Improving corrosion resistance and biocompatibility of AZ31 magnesium alloy by ultrasonic cold forging and micro-arc oxidation. *J. Biomater. Appl.* **2022**, *36*, 1664–1675. [CrossRef]
30. Elmensouri, G.; Kara, I.; Ahlatçi, H.; Türen, Y. Wear Resistance of Sheet Magnesium Alloy AZ31 with Micro Arc Oxidation Coatings After Shot Peening. *Met. Sci. Heat Treat.* **2021**, *63*, 426–429. [CrossRef]
31. Liu, S.Q.; Chen, J.H.; Zhang, D.D.; Wang, Y.X.; He, Z.; Guo, P.Y. Properties of Micro-Arc Oxidation Coatings on 5052 Al Alloy Sealed by SiO_2 Nanoparticles. *Coatings* **2022**, *12*, 373. [CrossRef]
32. Yu, Y.X.; He, B.L.; Lv, Z.M.; Lei, S.Y.; Xia, S.S. Experimental Research on Microhardness and Wear Resistance of MB8 Magnesium Alloy Treated by Ultrasonic Impact. *Rare Met. Mater. Eng.* **2017**, *46*, 1798–1802.
33. Luo, J.M.; Chen, Y.H.; Huang, J.; Xu, J. Effect of shot peening and micro-arc oxidation on microstructure and fatigue properties of TC4 titanium alloy. *Trans. Nonferrous Met. Soc. China* **2019**, *29*, 1210–1218.
34. Wang, C.H.; Li, R.F.; Bi, X.L.; Yuan, W.Y.; Gu, J.Y.; Chen, J.; Yan, M.J.; Zhang, Z.Y. Microstructure and wear resistance property of laser cladded CrCoNi coatings assisted by ultrasonic impact treatment. *J. Mater. Res. Technol.* **2022**, *22*, 853–864. [CrossRef]
35. Zhang, J.; Jian, Y.; Zhao, X.; Meng, D.; Pan, F.S.; Han, Q.Y. The tribological behavior of a surface-nanocrystallized magnesium alloy AZ31 sheet after ultrasonic shot peening treatment. *J. Magnes. Alloys* **2021**, *9*, 14. [CrossRef]
36. Amanov, A.; Penkov, O.V.; Pyun, Y.S.; Kim, D.E. Effects of ultrasonic nanocrystalline surface modification on the tribological properties of AZ91D magnesium alloy. *Tribol. Int.* **2012**, *54*, 106–113. [CrossRef]

37. Zhilyaev, A.P.; Shakhova, I.; Belyakov, A.; Kaibyshev, R.; Langdon, T.G. Wear resistance and electroconductivity in copper processed by severe plastic deformation. *Wear* **2013**, *305*, 89–99. [CrossRef]
38. Khorasanian, M.; Dehghan, A.; Shariat, M.H.; Bahrololoom, M.E.; Javadpour, S. Microstructure and wear resistance of oxide coatings on Ti-6Al-4V produced by plasma electrolytic oxidation in an inexpensive electrolyte. *Surf. Coat. Technol.* **2011**, *206*, 1495–1502. [CrossRef]
39. Leng, Z.J.; Li, T.; Wang, X.T.; Zhang, S.Q.; Zhou, J.X. Effect of Graphite Content on the Conductivity, Wear Behavior, and Corrosion Resistance of the Organic Layer on Magnesium Alloy MAO Coatings. *Coatings* **2022**, *12*, 434. [CrossRef]
40. Guo, P.; Tang, M.; Zhang, C. Tribological and corrosion resistance properties of graphite composite coating on AZ31 Mg alloy surface produced by plasma electrolytic oxidation. *Surf. Coat. Technol.* **2018**, *359*, 197–200.
41. Chen, C.; Zhang, H. Characteristics of friction and wear of Al-Zn-Mg-Cu alloy after application of ultrasonic shot peening technology. *Surf. Coat. Technol.* **2021**, *423*, 127615. [CrossRef]
42. Li, Y.; Lian, Y.; Jing, F.; He, T.; Zou, Y. Improvement in the tribological behaviour of surface-nanocrystallised 304 stainless steel through supersonic fine particle bombardment. *Appl. Surf. Sci.* **2023**, *627*, 157334. [CrossRef]

Disclaimer/Publisher's Note: The statements, opinions and data contained in all publications are solely those of the individual author(s) and contributor(s) and not of MDPI and/or the editor(s). MDPI and/or the editor(s) disclaim responsibility for any injury to people or property resulting from any ideas, methods, instructions or products referred to in the content.